THE ASTROPHYSICAL JOURNAL, 307:313–323, 1986 August 1

CO LINE FORMATION IN BIPOLAR FLOWS. I. ACCELERATED OUTFLOWS

SYLVIE CABRIT
Institut d'Astrophysique de Paris; and Ecole Normale Supérieure, Paris

AND

CLAUDE BERTOUT
Institut d'Astrophysique de Paris; and Laboratoire d'Astrophysique Théorique du Collège de France
Received 1985 August 19; accepted 1986 January 14

ABSTRACT

This paper investigates CO line formation in accelerated and constant velocity bipolar outflows. Depending on the view angle and the flow's opening angle, four different classes of characteristic line profiles, velocity versus position maps, and integrated intensity maps can be distinguished. We then use our models to test the most common method for deriving parameters of the flow from observed CO maps and find it to be inaccurate, mainly because in most cases it underestimates both the CO column density and the flow's characteristic time scale. Some suggestions for improved accuracy follow.

Subject headings: interstellar: molecules — line formation — stars: pre–main-sequence — stars: winds

I. INTRODUCTION

The discovery of high-velocity molecular flows in the vicinity of young stellar objects (Snell, Loren, and Plambeck 1980; Edwards and Snell 1982; Bally and Lada 1983; and others) is widely regarded as a major advance in the ongoing research on pre–main-sequence evolution, mainly because bipolar molecular outflows can apparently be driven by embedded pre–main-sequence OB stars as well as by low-luminosity, T Tauri–like objects, which in turn suggests that bipolar mass ejection is a universal phase of pre–main-sequence evolution. And a recent paper by Mundt *et al.* (1985), which reveals that L1551 IRS 5's optical spectrum resembles that of a FU Orionis object, brings together three of the most exciting aspects of stellar formation, namely bipolar CO flows, optical jets, and the FU Orionis phenomenon.

Observations of high-velocity molecular flows (HVMFs) lead one to ask both how they are powered and what the collimation mechanism responsible for the bipolar nature of many HVMFs may be. Snell, Loren, and Plambeck (1980) proposed a qualitative model in which the CO gas is accelerated outward by a collimated stellar wind while remaining confined to a shell surrounding the wind bubble. Pudritz and Norman (1983), Pudritz (1985), and Uchida and Shibata (1984, 1985) suggest instead that the molecular gas is a low-temperature centrifugally driven outflow emerging from an accretion disk; in this picture, outflow occurs along hourglass-shaped surfaces. A third model, in which the molecular material is set in motion by viscous coupling to a gaseous jet, is presently under investigation (R. N. Henriksen, private communication). In the latter, CO emission occurs in most of both lobes' volume. Several wind collimation mechanisms, which differ by the scale on which collimation occurs, have also been discussed. For example, Sakurai (1985) proposes a process intrinsic to the magnetized star, while Königl (1982) advocates collimation on a much larger, interstellar scale.

While the theoretical problems arising from observations of molecular outflows have been so widely addressed, leading to a number of possible models, little has been done so far to exploit the wealth of information contained in the observed CO line profiles, although such analysis could potentially allow one to choose between these various models. This paper, the first in a series exploring velocity fields and CO excitation conditions in bipolar outflows, represents a step in that direction. We developed a computer code which allows for the computation of NLTE CO line formation in bipolar geometry and in the presence of velocity fields. In this paper, we parameterize velocity fields and hydrogen density distributions, and we investigate CO emission originating from two biconical lobes in the presence of accelerating radial outflows. Because observed CO line profiles do not show the double-peak structure which would be expected if the emitting cones were only partially filled up (see also Levreault 1985), we assume in the following that the CO gas fills up the lobes, in contrast to some of the models mentioned above. Our main goal at this stage is not to set constraints on theoretical models, but rather to analyze and quantify uncertainties arising while deriving CO flow parameters from observed maps. Our code can, however, handle arbitrary axially symmetric velocity fields and H_2 densities; and forthcoming papers will be dedicated to the study of proposed models for the CO outflows.

Our computational method is explained in § II, results are presented in § III for two velocity fields, and § IV assesses the validity of the method used by observers to derive, in particular, the momentum rate in the CO flow and the stellar mass loss rate. This study has led us to doubt that accurate stellar mass loss rates can be derived at this point from observations of CO outflow associated with the star; but it did help identify points of uncertainty, so that we can suggest ways to improve the situation.

II. METHOD

The geometry of the model is shown in Figure 1. The molecular gas is confined to a bicone of opening angle $\theta_{\max}$, inner radius $r_{\min}$, and outer radius $r_{\max} = \sigma r_{\min}$. For this exploratory study, we restricted ourselves to power-law velocity fields

$$\boldsymbol{v}(r) = v_{\min}(r_{\min}/r)^{\alpha}\boldsymbol{u} , \quad (1)$$

where $\boldsymbol{u} = \boldsymbol{r}/r$, and we consider only accelerated and constant velocity outflows with $\alpha \leq 0$ and $v_{\min} > 0$. Mass conservation

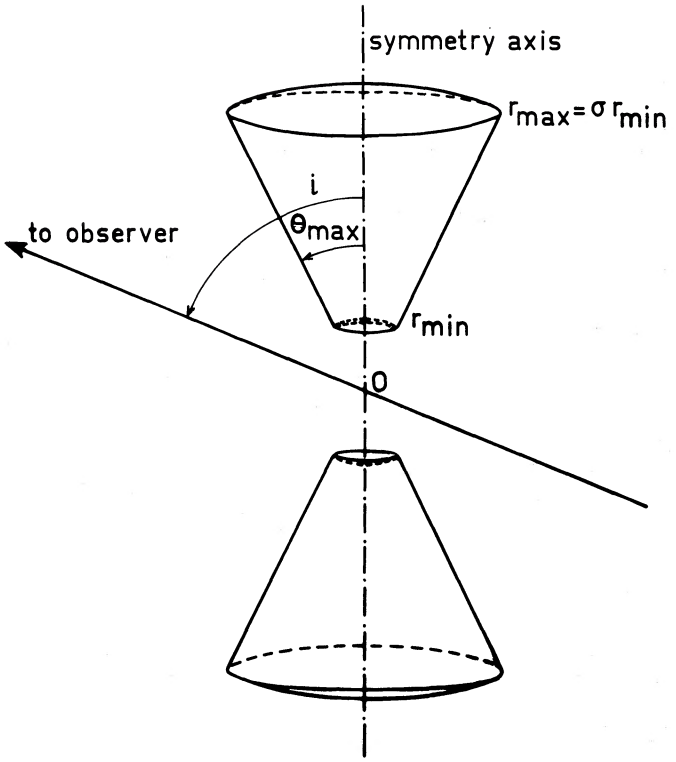

FIG. 1.—Geometry of the model

is assumed within the flow, so that the density $n(r)$ is given by

$$n(r) = n(r_{\rm min})(r_{\rm min}/r)^{\delta}\,, \tag{2}$$

with $\delta = 2 - \alpha$. We further assume that a star of radius r_c located at the symmetry center emits isotropic blackbody radiation at effective temperature T_c.

Bastian *et al.* (1980) and Hamann (1981) have demonstrated that an approach to the line formation problem using the Sobolev (1957) approximation for computing the level populations, but integrating the profiles exactly, gives excellent results for fast flows. We use this approach in the following.

a) CO *Excitation*

In the conditions typical of interstellar clouds, where CO molecules are heated both by the microwave background emission at $T_b = 2.7$ K and by collisions with H_2 molecules at a kinetic temperature T_k of typically 10 K, only the rotational sublevels of the ground electronic and vibrational state of CO are significantly populated. Each rotational level has energy $E_j = hB_0 j(j+1)$, where $B_0 = 57.6$ GHz and where $g_j = 2j + 1$ is the level degeneracy. Neglecting the effects of dust on CO excitation, the two main processes which contribute to populating these levels are radiative transitions and collisions with H_2 molecules.

The rate of change in the statistical population n_j of level j resulting from spontaneous and stimulated radiative transitions is

$$(dn_j/dt)_{\rm rad} = n_{j+1}A_{j+1,j} + (n_{j+1}B_{j+1,j} - n_j B_{j,j+1})\bar{J}_j - n_j A_{j,j-1} - (n_j B_{j,j-1} - n_{j-1}B_{j-1,j})\bar{J}_{j-1}\,, \tag{3}$$

where $\bar{J}_j(r)$ denotes the mean intensity integrated over the local profile for the transition j to $j+1$ at frequency $\nu_j = 2hB_0(j+1)$:

$$\bar{J}_j \equiv \left(\frac{1}{4\pi}\right)\int_0^{\infty} d\nu \int_{4\pi} d\Omega(\boldsymbol{n})\Phi\left[\nu - \nu_j - \nu_j\frac{(\boldsymbol{v}\cdot\boldsymbol{n})}{c}\right] I(\nu, \boldsymbol{n})\,. \tag{4}$$

Since we consider expansion velocities much greater than the CO local velocity dispersion, the radiation field remains essentially local; either each photon is reabsorbed in the immediate vicinity of its emission point, or it escapes from the flow, having been Doppler-shifted in the other molecules' rest frame. This simplifying fact was first used by Sobolev (1957). Extending the same formalism to our case, we find

$$\bar{J}_j = (1 - \beta_j)S_j + \beta_j^c B(\nu_j, T_c) + (\beta_j - \beta_j^c)B(\nu_j, T_b)\,, \tag{5}$$

where S_j, the source function for transition j, is

$$S_j = 2h\nu_j^3/c^2[(2j+3)n_j/(2j+1)n_{j+1} - 1]^{-1}\,. \tag{6}$$

Here, β_j is the total local escape probability, and β_j^c the escape probability reduced to the solid angle Ω_c within which the emitting core is seen from r. Expressions for β_j and β_j^c in axial geometry are found in, e.g., Bertout (1979).

With equations (1) and (2), the line center optical depth for line j in direction $\boldsymbol{n}$ can be written

$$\tau_j = k(r)(j+1)(x_j - x_{j+1})[1 - (1+\alpha)(\boldsymbol{u}\cdot\boldsymbol{n})^2]^{-1}\,, \tag{7}$$

where $k(r)$ is given by

$$k(r) = (8\pi^3\mu^2/3h)n_{\rm CO}(r)r/v(r) = k(r_{\rm min})(r_{\rm min}/r)^{1-2\alpha} \tag{8}$$

and where, following Goldreich and Kwan (1974), we define $x_j(r)$, the normalized level population, as

$$x_j(r) = (1/g_j)n_j(r)/n_{\rm CO}(r)\,. \tag{9}$$

The radiative rate of change for x_j is thus

$$(dx_j/dt)_{\rm rad} = A_{j+1,j}(2j+3/2j+1)[\![\beta_j x_{j+1} + (x_{j+1} - x_j) \times \{\beta_j^c/[\exp(h\nu_j/kT_c) - 1] + (\beta_j - \beta_j^c)/[\exp(h\nu_j/kT_b) - 1]\}]\!] - A_{j,j-1}[\![\beta_{j-1}x_j + (x_j - x_{j-1})\{\beta_{j-1}^c/[\exp(h\nu_{j-1}/kT_c) - 1] + (\beta_{j-1} - \beta_{j-1}^c)/[\exp(h\nu_{j-1}/kT_b) - 1]\}]\!]\,. \tag{10}$$

With $C(i\rightarrow j)(r)$ denoting the probability of collisional transition between levels i and j averaged over the relative velocities at point r, we have

$$(2i+1)C(i\rightarrow j) = (2j+1)C(j\rightarrow i)\exp[-(E_j - E_i)/kT_k]\,, \tag{11}$$

and the collisional rate of change for x_j is

$$\left(\frac{dx_j}{dt}\right)_{\rm coll} = \sum_{i\neq j}\left\{x_i\exp\left[-\frac{(E_j - E_i)}{kT_k}\right] - x_j\right\}C(j\rightarrow i)\,. \tag{12}$$

We shall assume that statistical equilibrium has been established in the flow, i.e., that

$$(dx_j/dt)_{\rm rad} + (dx_j/dt)_{\rm coll} = 0\,. \tag{13}$$

For a molecule with N levels, we thus solve $N - 1$ coupled equations (given by eq. [13]) together with a conservation equation for the total number of molecules, using an iterative method; $\beta_j(r)$ and $\beta_j^c(r)$ are computed from starting values of the $x_j(r)$ (for example, the LTE values at $T = T_k$) and the system is then solved, which provides new estimates for the $x_j(r)$. This simple procedure converges because $\bar{J}_j$ is determined locally. Typically, 3–12 iterations are needed to reach a con-

vergence rate of 10^{-4}. The actual computations considered 6–10 rotational levels.

b) *Profiles and Maps*

Computation of the emergent intensity in the observer's direction is performed exactly, using the algorithm proposed by Bertout (1984) after suitable generalization to axial geometry according to the formalism developed in Bertout (1979). Doppler widening at the local kinetic temperature was assumed for computing the absorption profile's width in the comoving frame. Contour maps similar to those presented by observers of high-velocity molecular outflows are drawn once the line profiles have been obtained for all lines of sight. The map of velocity versus position presents line intensity contours as a function of both radial velocity and position along the flow axis projected onto the plane of the sky. The contribution of the static ambient cloud, which appears in the observed maps as vertical contours centered on zero radial velocity, is of course not present in our maps. In the integrated intensity maps, the antenna temperature is integrated separately over the positive and negative radial velocities of each profile, giving levels of constant blue and red integrated intensity. We computed a series of models corresponding to different flow geometries and to various values of the free parameters $k(r_{\min})$, the convenient optical depth parameter defined in eq. (8), n_{H_2} at $r_{\min}$, T_k, and α, the velocity law exponent.

III. RESULTS

a) CO *Excitation*

We tested our computer code by comparing numerical results to those of Goldreich and Kwan (1974); Goldsmith (1972); and Goldsmith, Young, and Langer (1983) and found in each case excellent agreement. In the actual computations, we used collision rates given by Green and Thaddeus (1976). Although CO excitation conditions are sensitive to the assumed values of the collision rates, Goldsmith, Young, and Langer (1983) have shown, and our tests confirmed, that disagreement between published collision rates was quite small and that resulting differences in CO excitation should not exceed 20%.

Maps of the ambient cloud emission often suggest that a heating source is present near the center of the molecular flows. We thus studied the influence of a central radiating source on excitation in the accelerated gas and, as expected, found that the source function at a point r increases with $\Omega_c I_c$, where Ω_c is the solid angle of the emitting core as seen from r. In the case of intermediate optical thickness [$k(r_{\min}) = 200$ and $n_{H_2}(r_{\min}) = 10^4$], this term will dominate the source function whenever $(T_c/2.7 \times 10^5 \text{ K})(r_c/10^4 \ R_\odot)^2 \approx (r_{\min}/10^{-2} \text{ pc})^2$. Since the observed values of $r_{\min}$ lie in the range 10^{-2} to 10^{-1} pc (Goldsmith, Snell, and Hemeon-Heyer 1984), we do not expect radiation from a central source to contribute significantly to HVMF excitation, even in the case of a high-luminosity embedded source.

b) *Profiles and Maps*

While line intensities depend mainly on the medium's physical conditions, both profiles and contour maps are affected more by the flow geometry and the view angle i. From Figure 1 we see that if $i \leq \pi/2 - \theta_{\max}$, emission from the front cone is entirely blueshifted, while the far cone is entirely redshifted; and if $i \leq \theta_{\max}$, both cones are on the line of sight. It therefore becomes convenient to distinguish four cases, shown in Table 1. The probability of observing the flow in a given configuration is shown in Figure 2.

TABLE 1

THE DIFFERENT GEOMETRICAL CASES IN A BICONICAL FLOW

First Cone Blueshifted, Second Cone Redshifted	Each Cone Partly Blue-, Partly Redshifted
Two Cones on the Line of Sight	
Case 1: $i < \theta_{\max}$, $i \leq \pi/2 - \theta_{\max}$	Case 4: $i < \theta_{\max}$, $i > \pi/2 - \theta_{\max}$
One Cone on the Line of Sight	
Case 2: $i \geq \theta_{\max}$, $i \leq \pi/2 - \theta_{\max}$	Case 3: $i \geq \theta_{\max}$, $i > \pi/2 - \theta_{\max}$

Figures 3–6 correspond to the same flow geometry (with $\theta_{\max} = 30°$) and illustrate cases 1, 2, and 3. In each figure, four panels are displayed. The first one shows the line temperature for the sight line which crosses the flow closest to the symmetry center, plotted as a function of the normalized radial velocity $x \equiv v_{\text{rad}}/v(r_{\max})$, for two velocity fields ($\alpha = -1$ and $\alpha = 0$). The line temperature is defined by

$$T_l(v) \equiv c^2/2kv^2[I(v) - B(v, T_b)] .$$

The second panel then displays maps of velocity versus position for both velocity fields, and the last two panels show the corresponding integrated intensity maps. In all maps, positions in the plane of the sky are given by offsets from the center, in units of $r_{\min}/4$. Other parameters entering the computations have the following values, meant to represent a typical molecular outflow: $n_{H_2}(r_{\min}) = 10^4 \text{ cm}^{-3}$, $T_k = 10$ K, $A(^{12}\text{CO}) = 40A(^{13}\text{CO}) = 8 \times 10^{-5}$ (where the ^{13}CO abundance is from Dickman 1978), $r_{\min} = 0.06$ pc, $\sigma = 10$, and $v(r_{\max}) = 10 \text{ km s}^{-1}$.

Figure 3 (with $i = 5°$) corresponds to case 1 above. The profiles have two components, representing the cone emission on each side of zero radial velocity. The influence of the velocity field is better illustrated in the velocity versus position map. Because of the lack of small projected flow velocities when $\alpha = 0$, profiles have narrow components ($\delta x \approx 0.2$) separated by a large gap ($x_{\min} \approx 0.8$) in that case, while for $\alpha = -1$ we find broad line wings ($\delta x \approx 0.5$) and a small gap ($x_{\min} \approx 0.1$). Since the two cones are seen nearly face-on, the blue and red contours of integrated intensity are circular and overlapping.

One striking feature found in all cases is that emission is always more intense in the red than in the blue, although our model is symmetrical. But this can be understood as the result of absorption in the flow; blue-displaced photons emitted from the innermost, densest layers in the cone closest to the observer can be absorbed by overlying material, while red-displaced photons emitted from the densest layers of the cone farthest from the observer can escape freely in the observer's direction because of their Doppler shift. This property has been observed in most of the high-velocity flows mapped so far and has been used as an argument in favor of outflow by Bally and Lada (1983); our quantitative computations confirm this argument.

Figure 5 ($i = 50°$) illustrates case 2, and Figure 4 corresponds to the limiting case between cases 1 and 2. The line

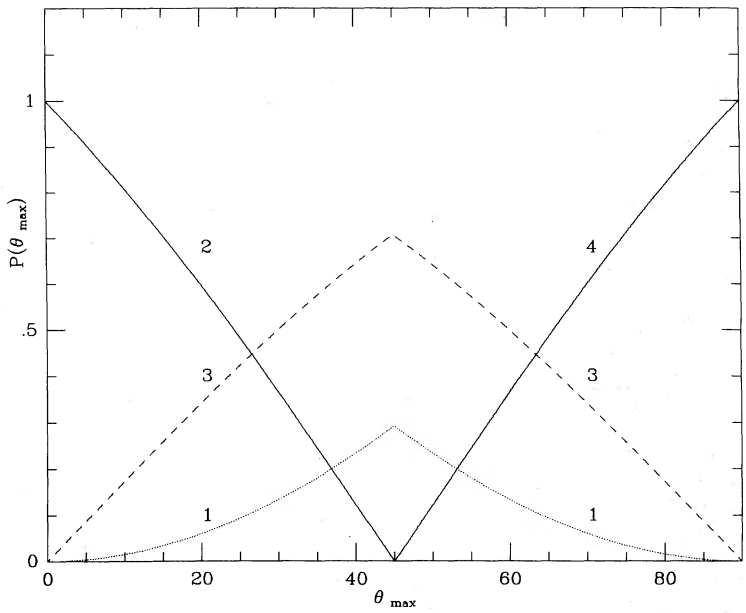

FIG. 2.—Probability $P(\theta_{max})$ of observing a biconical flow in each of the four configurations distinguished in the text as a function of θ_{max}

profiles are now completely asymmetrical. The range of radial velocities seen on the line of sight when $\alpha = 0$ increases with i, and the velocity versus position map for that case shows broad profiles over a velocity range ($\delta x \approx 0.6$) nearly independent of the position and comparable in extent to the central velocity gap ($x_{min} = 0.4$). For $\alpha = -1$, the line profile decreases more steeply and extends only over the lower part of the velocity range ($\delta x \approx 0.3$, $x_{min} = 0$), corresponding to the innermost, densest parts of the flow, where CO emission is sizable (recall that H_2 density varies as r^{-3} when $\alpha = -1$, and as r^{-2} when $\alpha = 0$). The blue and red emissions are formed in distinct regions of the map, thus revealing the bipolar structure of the flow. A central region, extending up to a projected distance $r_g = r_{min} \sin(i - \theta_{max})$ from the center of the flow, shows no emission. Such a gap has been observed in several high-velocity flows, for example in B335 (Goldsmith, Snell and Hemeon-Heyer 1984).

Case 3 is illustrated by Figure 6 (where $i = 80°$). Profiles have a single component extending from negative to positive radial velocities, while the intensity remains fairly constant over this range. The velocity versus position map indicates a maximum velocity extent of $x_{max} = 0.3$ for $\alpha = -1$ and $x_{max} = 0.6$ for $\alpha = 0$ (again with very flat profiles). The integrated intensity map again shows two distinct lobes, but each one now has a blue and a red component.

Although case 3 is the most probable one whenever $\theta_{max} > 30°$ (see Fig. 2), no example of it has been observed as yet. Several reasons could explain the lack of detection. First, emission at low radial velocities is indistinguishable from the ambient cloud contribution, so that case 3 flows might be classified as case 2 after subtraction of the central low-velocity emission. Second, most bipolar flows might have opening angles smaller than 30°. Finally, some observed flows with mixed blue and red emission, which are thought to be two separate outflows, could in fact represent a single case 3 bipolar flow; the CO emission discovered by Edwards and Snell (1984) near RNO 43 is a case in point.

Case 4 is a superposition of cases 1 and 3. We thus show in Figure 7 only an example of the rather complex integrated intensity map corresponding to that case, with $i = 50°$ and $\theta_{max} = 60°$. No flow showing this geometrical aspect has been detected so far, indicating either that the flows are well collimated ($\theta_{max} \leq 45°$) or that the attainable velocity resolution is not high enough.

IV. DISCUSSION

Bally and Lada (1983) emphasized that CO flow momentum rates derived from observations are often much higher than the maximum force supplied by the star to a radiatively driven wind, even for high-luminosity sources. While this result may indicate that other mechanisms, such as rotation, drive the CO flows, its reliability is critically dependent on the validity of the various assumptions (discussed by Lada 1985) underlying the derivation of the flow's momentum rate from observed maps. The same objection applies to computations of stellar mass loss rates based on the assumption that the high-velocity CO gas is accelerated by a stellar wind. In this case, the rate of momentum at the base of the flow $\dot{P}(r_{min})$ is related to the rate of momentum carried in the wind by $\dot{P}(r_{min}) = \epsilon \dot{M} V_{wind}$, where ϵ is the efficiency of the interaction, $\dot{M}$ the stellar mass loss rate, and V_{wind} the wind's end velocity. This assumption has been used by Edwards and Snell (1982) and Calvet, Cantó, and Rodríguez (1983) to derive mass loss rates for low-luminosity, T Tauri–like stars, whose wind-driving mechanisms are still an issue. One would therefore like to assess the usefulness of this method for deriving accurate mass loss rates.

The model presented in this paper is obviously still too crude to offer anything approaching a true and accurate representation of the observed flows. It cannot take the influence of clumps within the flow into account, although the low beam-filling factor noted by Plambeck, Snell, and Loren (1983) may suggest their presence in several molecular outflows. Neither does it consider the possible effect of shocks within the flow on the CO excitation. And as far as the biconical geometry of the flow and the power-law velocity fields are concerned, they are likely to be rather poor representations of the actual flow geometry and velocities. Our model, therefore, can only be a first approximation of the physical situation.

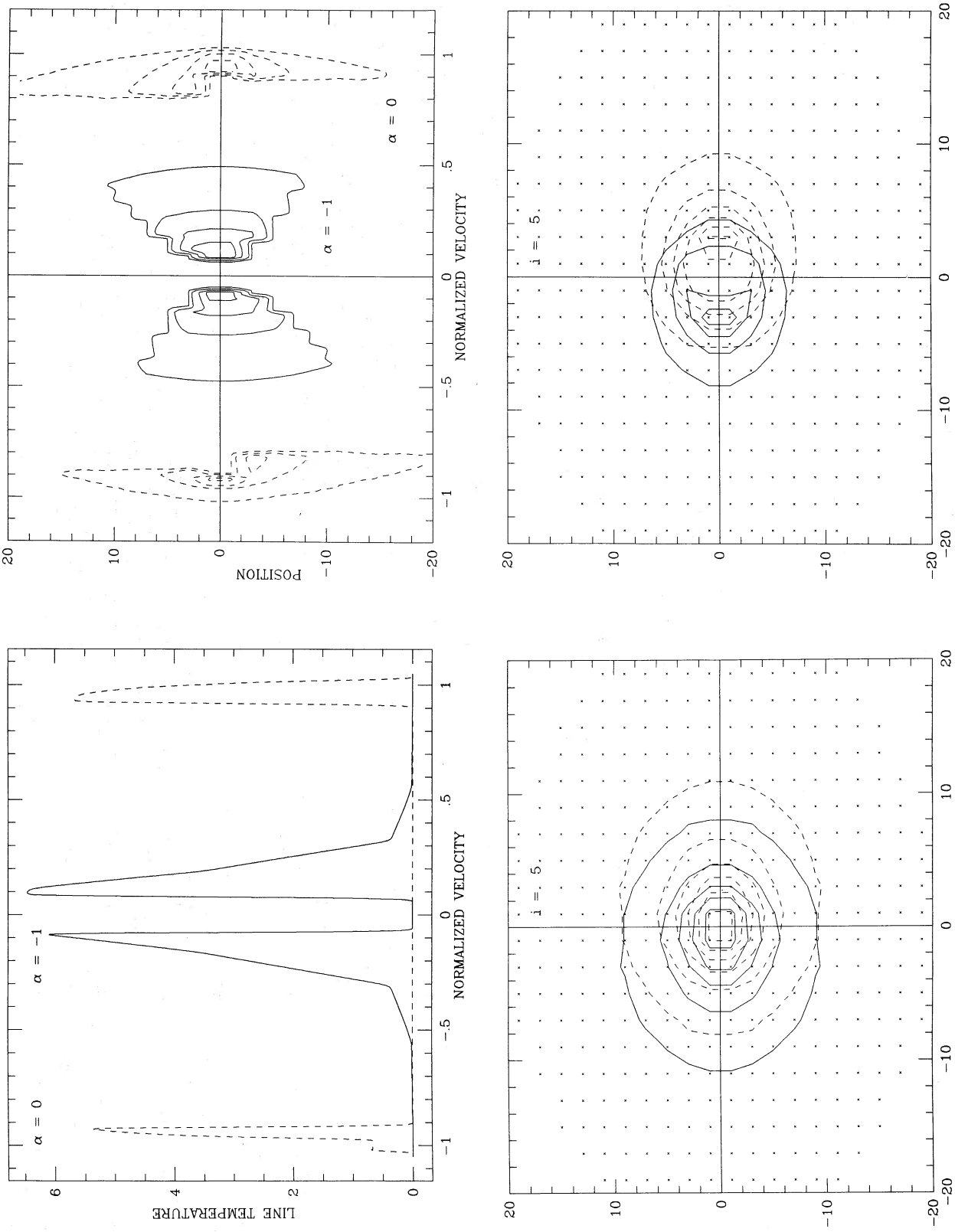

FIG. 3.—Results for a cone opening angle of 30° and an inclination angle $i = 5°$, corresponding to case 1 (see text for details and for the values of other parameters). (*upper left*) Profiles of the ^{12}CO $J = 1 \rightarrow 0$ line for the sight line crossing the molecular flow closest to the stellar core. The solid line is for case $\alpha = -1$, the dashed line for $\alpha = 0$. (*upper right*) Velocity vs. position map, showing contours of constant line temperature for $\alpha = -1$ (*solid lines*) and $\alpha = 0$ (*dashed lines*). Lowest contour level, 0.1 K; second one, 1 K; step between other contours, 2 K. Offsets in units of $r_{min}/4$. (*lower left*) Map of blue (*solid lines*) and red (*dashed lines*) integrated intensity for $\alpha = -1$. Emergent intensities computed at positions indicated by crosses. Contour levels (in K km s^{-1}) and distance scale as in upper right panel. (*lower right*) Same as lower left for $\alpha = 0$. Lowest contour level, 1 K km s^{-1}; second one, 5 K km s^{-1}; step between other contours, 5 K km s^{-1}.

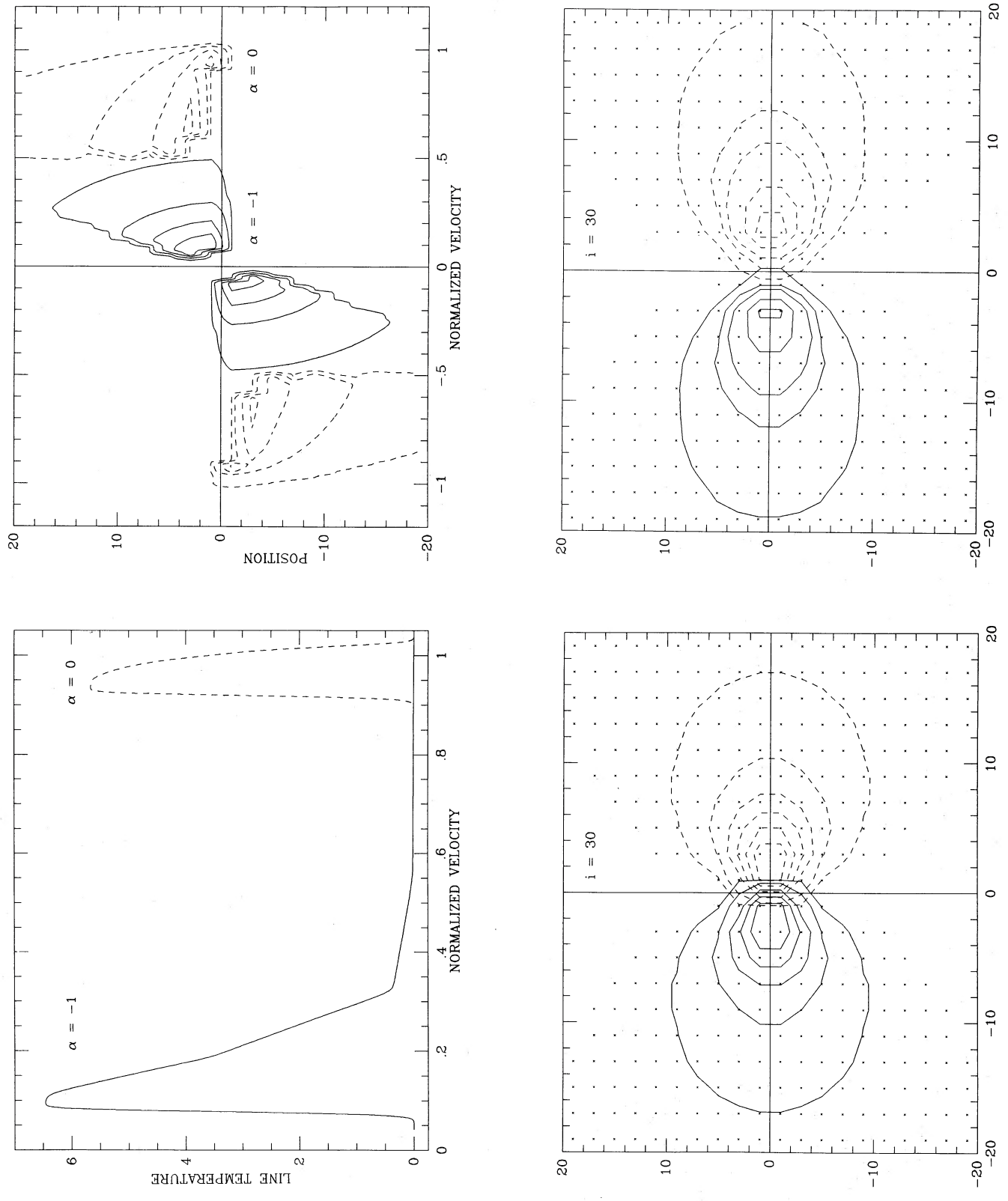

FIG. 4.—Same as Fig. 3, for $i = 30°$

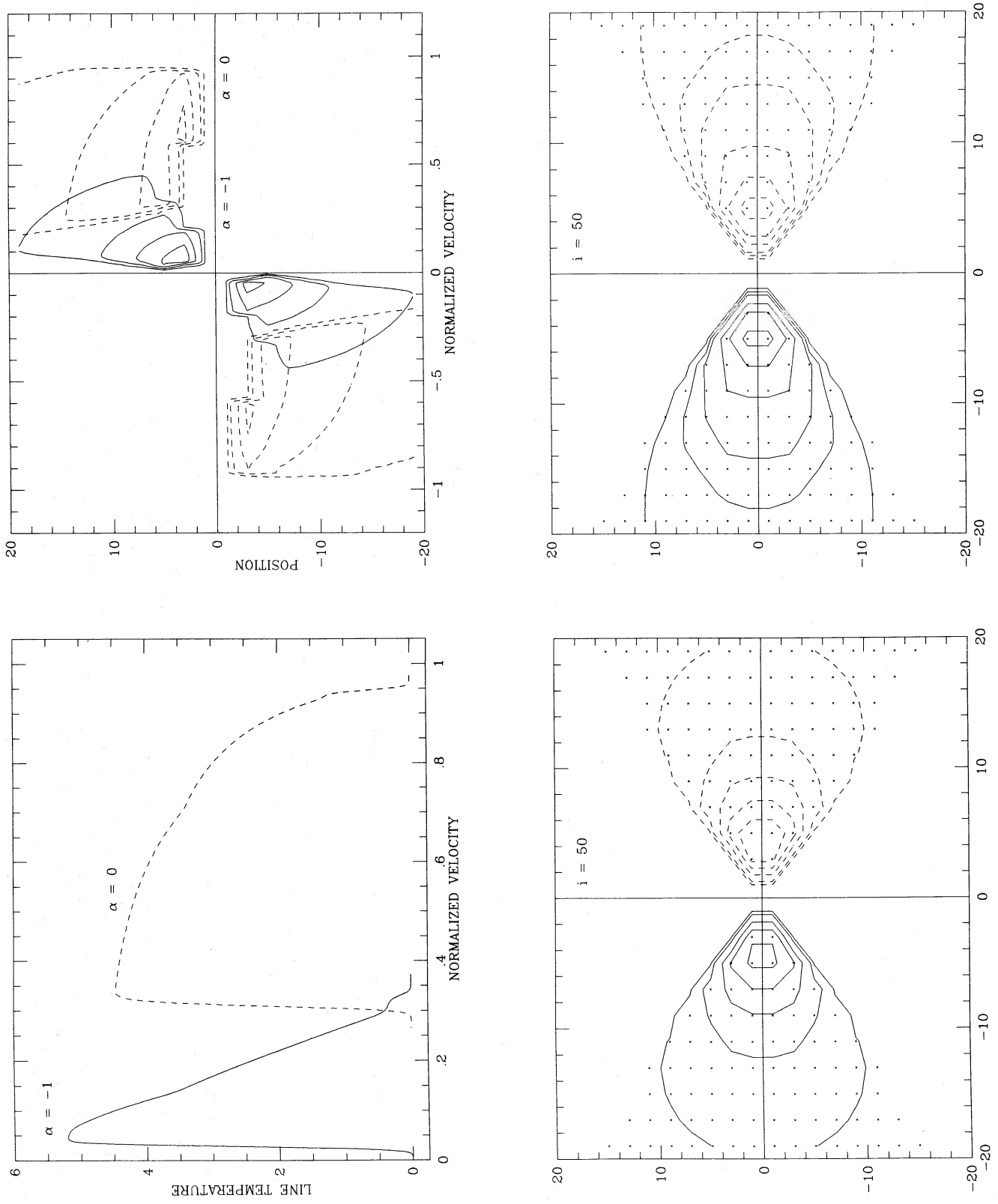

FIG. 5.—Same as Fig. 3, for $i = 50°$ (case 2)

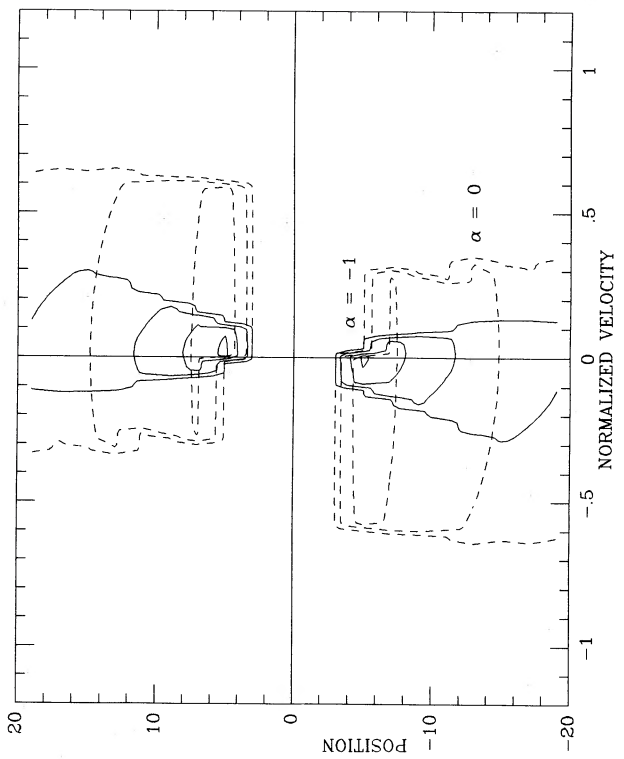

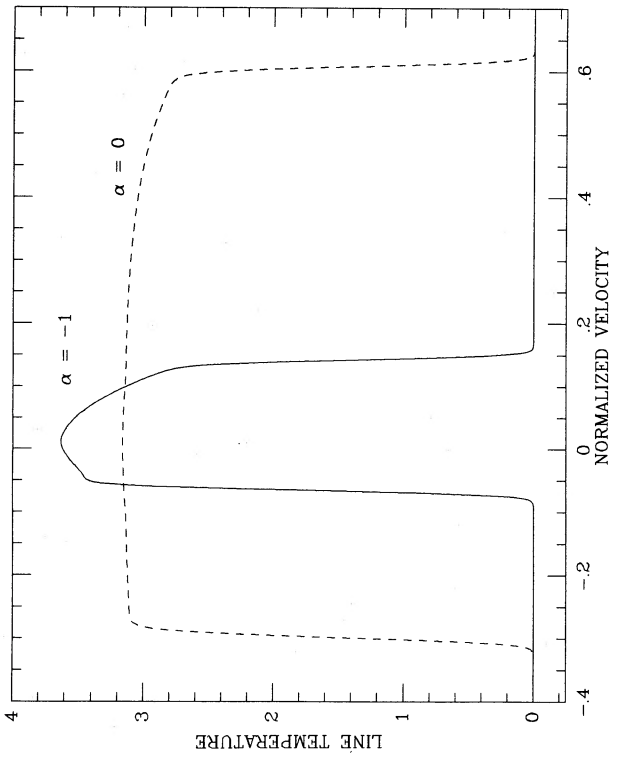

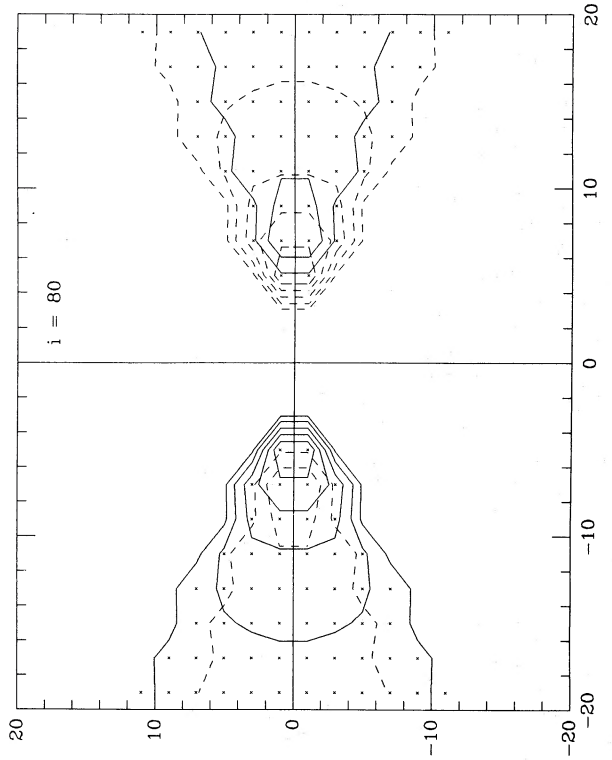

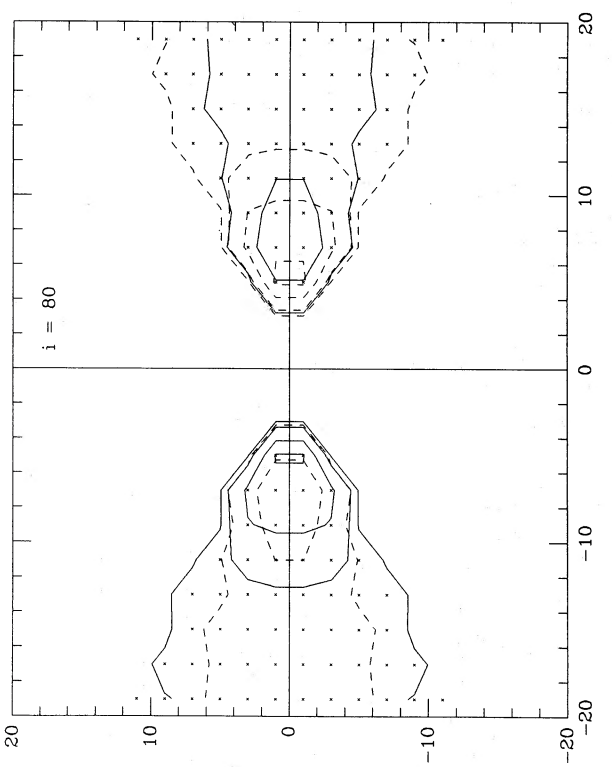

FIG. 6.—Same as Fig. 3, for $i = 80°$ (case 3)

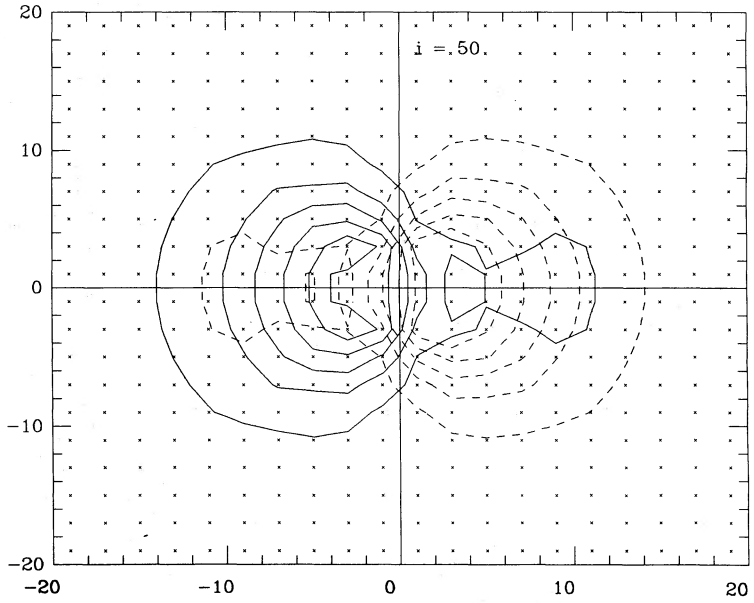

FIG. 7.—Integrated intensity map for $\theta_{max} = 60°$, $i = 50°$, and $\alpha = -1$, corresponding to case 4. Lowest contour level, 0.8 K km s^{-1}; second one, 3 K km s^{-1}; step between other contours, 2 K km s^{-1}.

But no matter how crude, the model investigated here allows one to test the method commonly used by observers, who derive various properties of the flows from the CO maps, against a model flow with known properties, making it possible for the first time to analyze quantitatively the various causes of error in the observers' standard method and their respective importance in the determination of the flow parameters and of the inferred stellar mass loss rate.

In the model discussed above, the actual values of the CO column density $N(\mathrm{CO})_c$ (in cm^{-2}), the flow's mass M_c (in $M_\odot$), the flow's momentum P_c (in $M_\odot$ km s^{-1}), and the flow's momentum rate at $r = r_{min}$ $\dot{P}_c$ (in $M_\odot$ km s^{-1} yr^{-1}) are given by

$$N(\mathrm{CO})_c = \int n_{\mathrm{CO}}(s)ds \,, \tag{14}$$

$$M_c = 0.6157 n_{\mathrm{H_2}}(r_{min}) r_{min}^3 (1 - \cos\theta_{max}) f(\sigma) \,, \tag{15}$$

$$P_c = M_c V_c \,, \tag{16}$$

$$\dot{P}_c(r_{min}) = 1.0374 \times 10^{-6} P_c/T_c \,, \tag{17}$$

where $f(\sigma) = \sigma - 1$ if $\alpha = 0$ or $\ln(\sigma)$ if $\alpha = -1$, $V_c = v_{min}(\sigma - 1)/f(\sigma)$ is the flow's characteristic velocity in km s^{-1}, and $T_c = (\sigma - 1) r_{min}/v_{min}$ is the flow's characteristic time scale in pc km^{-1} s.

The method commonly used by observers to derive the flow's parameters is based on the following expression for the velocity-integrated optical depth in the $J = 1 \rightarrow 0$ transition:

$$\int \tau_o(v)dv = \frac{8\pi^3\mu^2}{3h} \int x_o(1 - e^{-h\nu_o/kT_{ex}}) n_{\mathrm{CO}}(s)ds \,, \tag{18}$$

which can be transformed into the following relationship between integrated line temperature and total CO column density by introducing average values over the line of sight and the velocity profile:

$$\int T_l(v)dv = \left\langle \frac{1 - e^{-\tau_o}}{\tau_o} \right\rangle \langle J(T_{ex}) - J(T_b) \rangle \langle x_o(1 - e^{-h\nu_o/kT_{ex}}) \rangle \times \frac{N(\mathrm{CO}) 8\pi^3\mu^2}{3h} \,. \tag{19}$$

Here, the difficulty lies in evaluating the averaged (bracketed) quantities. The basic assumptions are that the line is optically thin, that LTE holds everywhere, and that the kinetic temperature in the flow is constant. Usually, this procedure is only applied to the line profiles observed at the flow's center, which are considered to be representative of the whole flow region. The resulting CO column density is then used to derive the flow's parameters according to

$$M_o = N_o m_{\mathrm{H_2}} \Sigma_o / A(\mathrm{CO}) \,, \tag{20}$$

$$P_o = M_o V_o \,, \tag{21}$$

$$\dot{P}_o = P_o/T_o \,, \tag{22}$$

where Σ_o, the projected surface of the flow; V_o, the maximum radial velocity; and $T_o = R_o/V_o$, the dynamical time scale of the flow, are all measured on the maps.

We thus computed the ratios of these quantities as determined using the standard observers' method (subscript o) to the same quantities computed according to equations (14)–(17) (subscript c). Tables 2 and 3 summarize results for the two velocity fields $\alpha = 0$ and $\alpha = -1$ and for several values of the view angle i. Values of the different computation parameters are given in the tables. Note that results of this comparison depend on $A(\mathrm{CO}) r_{min}/v_{min}$ rather than on the individual values of $A(\mathrm{CO})$, v_{min}, and r_{min}. The various sources of error in the determination of the flow's parameters when applying the standard method to accelerated and constant velocity outflows are discussed below.

Assuming that the transition is optically thin underestimates the ^{12}CO density by a factor of 1/2 to 1/20. Since $T_{ex} < T_k$, the second bracket in equation (19) is always overestimated in the LTE approximation, and the third bracket is underestimated because the levels higher than $j = 2$ are always underpopulated even when the transition is nearly thermalized (see also Dickman 1978). The final result is an underestimate of the central CO *column density* by a factor of 1/30 at worst.

From the computed values of N_c and M_c (cf. eqs. [14] and [15]), we estimate a characteristic projected flow surface Σ_c

TABLE 2

COMPARISON OF THE ACTUAL MODEL PARAMETERS WITH VALUES DERIVED USING THE OBSERVERS' STANDARD METHOD

	$\alpha = 0$				$\alpha = -1$			
RATIO	$i = 5°$	$i = 30°$	$i = 50°$	$i = 80°$	$i = 5°$	$i = 30°$	$i = 50°$	$i = 80°$
N_o/N_c	0.03	0.11	0.16	0.35	0.11	0.11	0.11	0.11
Σ_o/Σ_c	1.53	1.11	0.89	0.74	2.11	3.98	2.10	1.63
M_o/M_c	0.04	0.13	0.15	0.26	0.24	0.46	0.22	0.18
V_o/V_c	1.00	1.00	1.00	0.70	1.28	1.28	1.28	0.77
P_o/P_c	0.04	0.13	0.15	0.18	0.31	0.59	0.29	0.14
T_o/T_c	0.33	0.44	0.55	0.79	0.04	0.08	0.08	0.15
$\dot{P}_o/\dot{P}_c$	0.13	0.29	0.26	0.23	6.98	6.67	3.23	0.95

NOTE.—Input data of computations: $\theta_{max} = 30°$, $\sigma = 10$, $T_k = 10$ K, $n_{H_2}(r_{min}) = 10^4$ cm^{-3}, $k(r_{min}) = 200$ for $\alpha = -1$ and $= 20$ for $\alpha = 0$, corresponding to moderate optical depths.

from

$$M_c = \Sigma_c N_c m_{H_2}/A(\mathrm{CO})\,; \qquad (23)$$

Σ_c can then be compared to Σ_o, the projected area measured on the CO map, which is used in the standard method to compute the CO *mass*. We find that Σ_c is ~ 3 times larger in the case $\alpha = 0$ than in the case $\alpha = -1$, because of the difference in density gradient. In contrast, the apparent surface measured on maps Σ_o is nearly the same in both cases. The quotient Σ_o/Σ_c is around unity for $\alpha = 0$ but can be as large as 3 for $\alpha = -1$. In most cases, the total mass is still underestimated due to the large error in the column density, but it can be overestimated by up to a factor of 2 in flows with small line optical depths. Error in the characteristic flow velocity V_c does not appear critical. Error in the CO *momentum* is thus generally of the same order of magnitude as the error in the CO mass.

Because of the limited sensitivity of available detectors, r_{max} is always underestimated in observations; as a result, high-velocity flows always appear less collimated than in reality. Since v_{min} is always overestimated in the presence of velocity gradients, the *dynamical time scale*, as derived from these quantities, is usually too small by a large factor in accelerated outflows ($\alpha < 0$): more than 20 at small view angles, and typically 2–8 at view angles larger than $\sim 40°$. The *rate of momentum* at the basis of the flow will thus be overestimated by similar factors. The constant velocity case ($\alpha = 0$) may appear more favorable for deriving $\dot{P}$, both because the density falls more slowly outward and because there is no radial velocity gradient in the flow; but one finds that $\dot{P}$ can be underestimated by a factor of up to 10 at small view angles, due mainly to the largely underestimated CO mass in that case.

Several additional uncertainties are introduced when deriving *stellar mass loss rates* from the CO rate of momentum. They stem from: A(CO), the CO abundance relative to H_2; ϵ, the efficiency of the wind to molecular gas momentum exchange; and V_{wind}, the terminal velocity of the wind, which strongly depends on the nature of the central source. That there are so many sources for error, as shown above, convinced us that deriving accurate mass loss rates from observations of high-velocity CO outflows remains impossible at this point. In order to illustrate this conclusion, we now apply the above results to a discussion of T Tauri's mass loss rate. Besides the difficulties discussed above, one has to deal with the multiplicity of T Tauri; the CO outflow could be driven either by the brightest optical component (T Tauri North) or by the radio source (T Tauri South). While previous investigators have attributed the CO flow to T Tauri North, the lack of CO outflows around most T Tauri stars (Levreault 1985) and similarities between the radio source T Tauri South and both IRS 5 in L1551 and the radio source exciting the Herbig-Haro objects HH 1 and HH 2 now suggest that the CO flow is more probably driven by T Tauri South. We briefly consider consequences of both possibilities.

The CO high-velocity flow in the vicinity of T Tauri is peculiar because one sees mainly blue-displaced molecular gas, suggesting that T Tauri is located in front of a dense molecular core (Edwards and Snell 1982). Maps of the CO flow further indicate that we see the outflow almost face-on, a condition hardly favorable to accurate derivation of the flow parameters (cf. Tables 2 and 3). CO line profiles are compatible with those of an accelerated outflow; assuming for the sake of illustration that $\alpha \approx -1$ and $\theta_{max} \approx 30°$, we find $k(r_{min}) > 150$ from the

TABLE 3

COMPARISON OF THE ACTUAL MODEL PARAMETERS WITH VALUES DERIVED USING THE OBSERVER'S STANDARD METHOD

	$\alpha = 0$				$\alpha = -1$			
RATIO	$i = 5°$	$i = 40°$	$i = 60°$	$i = 85°$	$i = 10°$	$i = 40°$	$i = 60°$	$i = 85°$
N_o/N_c	0.11	0.46	0.69	1.01	0.59	0.65	0.67	0.68
Σ_o/Σ_c	1.50	1.20	0.48	0.79	3.29	2.45	1.59	2.30
M_o/M_c	0.16	0.56	0.33	0.79	2.00	1.58	1.07	1.60
V_o/V_c	1.00	1.00	0.85	0.50	0.77	0.77	0.51	0.26
P_0/P_c	0.16	0.56	0.28	0.40	1.50	1.21	0.55	0.40
T_o/T_c	0.22	0.56	0.52	1.11	0.07	0.15	0.22	0.44
$\dot{P}_o/\dot{P}_c$	0.73	1.01	0.54	0.36	20.4	8.20	2.46	0.91

NOTE.—Input data of computations: $\theta_{max} = 30°$, $\sigma = 10$, $T_k = 20$ K, $n_{H_2}(r_{min}) = 5 \times 10^3$ cm^{-3}, $k(r_{min}) = 50$ for $\alpha = -1$ and $= 10$ for $\alpha = 0$, corresponding to low optical depths.

lower limit on the CO central column density derived by Edwards and Snell. We thus conclude that the transition is not optically thin, and Table 2 shows that the CO momentum rate is overestimated by a factor of ~ 7 in the case which comes closest to that of T Tauri's outflow.

We first consider that the CO flow is driven by T Tauri South. Unfortunately, the lack of information about the nature of this source precludes a detailed analysis. Even if its radio spectrum is interpreted as the signature of a hot wind (Schwartz 1984; but see also Bertout 1983 for a different view), we cannot derive a mass loss rate from the CO flow because we do not know the terminal velocity of the wind. If, however, the CO flow emerges directly from the central object, as suggested by Pudritz (1985) and Uchida and Shibata (1985), a mass loss rate of $\sim 2 \times 10^{-6}\ M_\odot\ \mathrm{yr}^{-1}$ is derived from Edwards and Snell's data after correction of the CO momentum rate and the velocity at $r_{\min}$.

If the CO flow is driven by T Tauri North's stellar wind, and if momentum is conserved at the base of the CO flow, then the inferred stellar mass loss rate from our model is $1.4 \times 10^{-8}\ M_\odot\ \mathrm{yr}^{-1}$, while the value of $\dot{M}$ found with the same parameters—in particular, the same CO/H_2 ratio of 5×10^{-5}—but found by using the standard method, is of the order $10^{-7}\ M_\odot\ \mathrm{yr}^{-1}$ (Edwards and Snell 1982; Levreault 1985). Using the probably more realistic value of 10^{-4} for A(CO) (Black and Willner 1984) brings the necessary mass loss rate down to $\dot{M} \approx 7 \times 10^{-9}\ M_\odot\ \mathrm{yr}^{-1}$, a value smaller than the one derived for T Tauri North from VLA data when assuming that its radio emission is thermal ($\dot{M} \approx 4.5 \times 10^{-8}\ M_\odot\ \mathrm{yr}^{-1}$; Schwartz *et al.* 1984). Similar results are found for $\theta_{\max} = 60°$. We thus conclude that the optical star's wind may be massive enough to drive the flow.

V. CONCLUSIONS

The above study suggests that the standard method for deriving flow parameters from observed maps can be improved in several respects. First, we agree with Lada (1985) that observations of ^{13}CO lines should be used whenever possible, both because the transitions are optically thin and because the abundance of ^{13}CO is better known than that of ^{12}CO (Dickman 1978). Second, our results do offer an effective, if approximate, procedure for removing the ambient cloud's contribution to the observed line profiles. One begins by using the maps to determine which of the four cases defined in § III*b* applies to a given observation. If case 1 or 2 applies, then the central range can be entirely excluded; but for cases 3 and 4, taking an average constant value of T_l over the central range gives a better approximation. Finally, we note that considering only the central line of sight leads to overestimating the total mass, while adding up the contribution of each line profile over the flow region would give a true lower limit to the CO mass. We expect these suggestions will remain valid when other velocity fields are investigated.

Section IV demonstrated how difficult it is to predict the HVMF's momentum rate from the observed maps, since the assumption of small optical depth can lead to underestimating the column density, while the underestimation of the flow extent results in characteristic time scales that can be much too small. Extreme caution must therefore be exercised when discussing the possible significance of CO outflow momentum rates and stellar mass loss rates inferred from HVMF observations until the physics of the CO outflows are better understood.

It is a pleasure to thank J. Adams for help in editing the text.

REFERENCES

Bally, J., and Lada, C. J. 1983, *Ap. J.*, **265**, 824.
Bastian, U., Bertout, C., Stenholm, L., and Wehrse, R. 1980, *Astr. Ap.*, **86**, 105.
Bertout, C. 1979, *Astr. Ap.*, **80**, 138.
———. 1983, *Astr. Ap.*, **126**, L1.
———. 1984, *Ap. J.*, **285**, 269.
Black, J. H., and Willner, S. P. 1984, *Ap. J.*, **279**, 673.
Calvet, N., Cantó, J., and Rodríguez, L. F. 1983, *Ap. J.*, **268**, 739.
Dickman, R. L. 1978, *Ap. J. Suppl.*, **37**, 407.
Edwards, S., and Snell, R. L. 1982, *Ap. J.*, **261**, 151.
———. 1984, *Ap. J.*, **281**, 237.
Goldreich, P., and Kwan, J. 1974, *Ap. J.*, **189**, 441.
Goldsmith, P. F. 1972, *Ap. J.*, **176**, 597.
Goldsmith, P. F., Snell, R. L., and Hemeon-Heyer, M. 1984, *Ap. J.*, **286**, 599.
Goldsmith, P. F., Young, J. S., and Langer, W. D. 1983, *Ap. J. Suppl.*, **51**, 203.
Green, S., and Thaddeus, P. 1976, *Ap. J.*, **205**, 766.
Hamann, W. R. 1981, *Astr. Ap.*, **93**, 353.
Königl, A. 1982, *Ap. J.*, **261**, 115.
Lada, C. J. 1985, *Ann. Rev. Astr. Ap.*, **23**, 267.
Levreault, R. M. 1985, Astronomy Dept., University of Texas, Austin, *Tech. Rept.*, No. 85-1.
Mundt, R., Stocke, J., Strom, S. E., Strom, K. M., and Anderson, E. R. 1985, *Ap. J. (Letters)*, **297**, L41.
Plambeck, R. L., Snell, R. L., and Loren, R. B. 1983, *Ap. J.*, **266**, 321.
Pudritz, R. E. 1985, *Ap. J.*, **293**, 216.
Pudritz, R. E., and Norman, C. A. 1983, *Ap. J.*, **274**, 677.
Sakurai, T. 1985, *Astr. Ap.*, submitted.
Schwartz, P. R., Simon, T., Zuckerman, B., and Howell, R. R. 1984, *Ap. J. (Letters)*, **280**, L23.
Snell, R. L., Loren, R. B., and Plambeck, R. L. 1980, *Ap. J. (Letters)*, **239**, L17.
Sobolev, V. V. 1957, *Soviet Astr.—AJ*, **1**, 678.
Uchida, Y., and Shibata, K. 1984, *Pub. Astr. Soc. Japan*, **36**, 105.
———. 1985, *NASA Conf. Pub.*, No. 2358, p. 169.

CLAUDE BERTOUT and SYLVIE CABRIT: Institut d'Astrophysique, 98 bis Bd Arago, F-75014 Paris, France